Impacts on thin elastic sheets

By Romain Vermorel, Nicolas Vandenberghe*
and Emmanuel Villermaux

IRPHE, CNRS-Aix Marseille Université, 49, rue Frédéric Joliot-Curie, 13384 Marseille Cedex 13, France

We study transverse impacts of rigid objects on a free elastic membrane, using thin circular sheets of natural rubber as experimental models. After impact, two distinct axisymmetric waves propagate in and on the sheet. First, a tensile wave travels at sound speed leaving behind the wavefront a stretched domain and then a transverse wave propagates on the stretched area at a lower speed. In the stretched area, geometrical confinement induces compressive circumferential stresses leading to a buckling instability, giving rise to radial wrinkles. We report on a set of experiments and theoretical remarks on the conditions of occurrence of these wrinkles, their dynamics and wavelength.

Keywords: membrane; impact; buckling; wrinkling

1. Introduction

When a thin elastic sheet is impacted transversely by a rigid body, it deforms locally out of its plane. Depending on the nature of the material and the strength of the impact, the sheet may be perforated, it may deform permanently or it may present radial or circumferential cracks (Backman & Goldsmith 1978). An understanding of these phenomena requires knowledge of the global response of a sheet to localized impacts.

Sheets with small thickness have a weak intrinsic bending rigidity. Very thin sheets such as clothes or biological membranes can thus freely bend and they often exhibit wrinkles (Cerda *et al.* 2004). If the sheet is stretched, this is no longer the case since any transverse motion is accompanied by a restoring force proportional to the tension. On the other hand, if the sheet is compressed, a buckling instability develops and the membrane wrinkles.

We consider the problem of a free-standing axisymmetric membrane impacted transversely at its centre. A static version of this problem, namely a membrane clamped at its boundaries deformed by a punctual force, has been considered by Begley & Mackin (2004). In this static configuration, the membrane remains axisymmetric for any force, with no wrinkling. When a free-standing membrane (i.e. a membrane with no initial stress) is impacted, tensile stresses develop as a

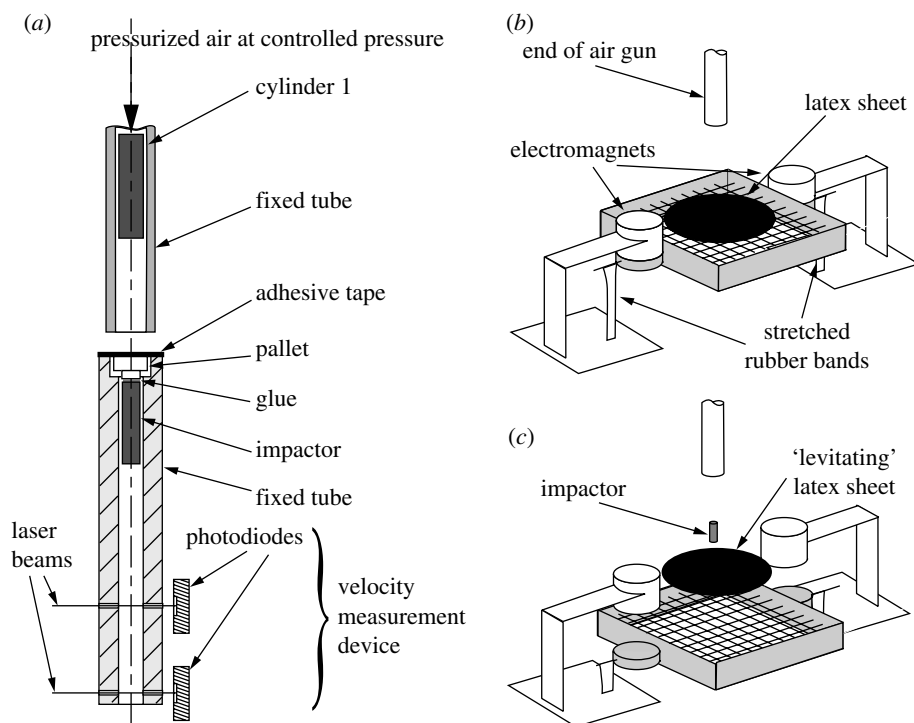*Author for correspondence (nvdb@irphe.univ-mrs.fr).

Figure 1. Experimental set-up: (*a*) a two-stage gas gun is used to launch impactors. When the cylinder 1 hits the pallet, the adhesive tape is torn off, the pallet is accelerated and the slightly glued impactor is released; (*b*) the impacted sheet stands on a netting stretched on a frame, and (*c*) when the gas gun is triggered, the electromagnets are switched off and the frame is pulled by two rubber bands. The impactor hits a free sheet.

result of the impact. This problem is more complicated than the classical drum problem (Graff 1975), in which the variation of in-plane stresses due to the impact itself are neglected. Phoenix & Porwal (2003) have reviewed previous results on the impacts on free-standing membranes in the context of fibrous system (e.g. textile, etc.). They also developed a model for the ballistic response of an axisymmetric free-standing membrane neglecting compressive circumferential stresses. However, as seen in figures 2 and 3, when a free-standing membrane is impacted, it buckles and radial wrinkles appear. The aim of this present work is to describe the sequence of events inducing this instability. We first describe the axisymmetric stress field resulting from the impact and we show that a region of the membrane experiences circumferential compression. We then study the development of the buckling instability leading to the formation of radial wrinkles, and we propose a model predicting their wavelength.

2. Experimental set-up

We use a vertical gas gun to launch steel cylinders and spheres of radius $r_i = 2.25$ mm (figure 1). Unless otherwise noted, steel cylinders of length 27 mm and mass 3.3×10^{-3} kg are used for the measurements. A cylinder is accelerated
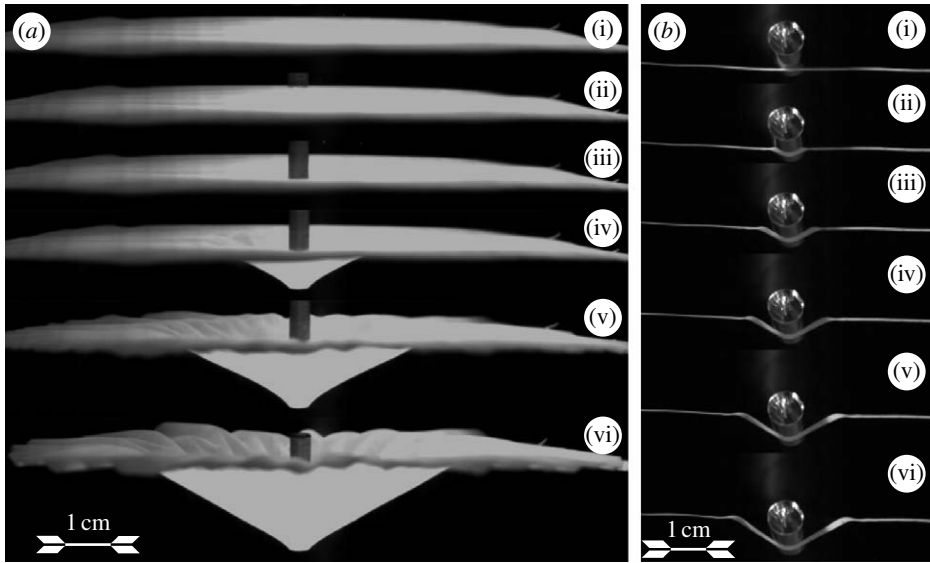
Figure 2. (*a*) Impact of a steel cylinder on a thin rubber sheet of radius $r_0=60$ mm and thickness $h=0.10$ mm. The time step between two frames is 1.33 ms. ((i)–(iii)) The cylinder of radius $r_i=2.25$ mm impacts the free levitating sheet at velocity $V=5.8$ m s^{-1}. (*iv*) After impact a cone expands. ((v)–(vi)) The propagation of both tensile and transverse waves yield an in-plane stress field that will eventually induce a buckling instability. A movie showing the dynamics is included in the electronic supplementary materials. (*b*) Impact of a free-falling rod on a thin rubber strip of thickness 0.10 mm, length 100 mm and width 4 mm. The time step between two frames is 0.50 ms. (*i*) The rod impacts the free levitating strip with velocity $V=3.7$ m s^{-1}. ((ii)–(vi)) After impact a V-shaped area expands.

by pressurized air inside a 40-cm-long tube. Beneath this tube stands a pallet to which we lightly glue the impactor (cylinder or sphere). As the cylinder hits the pallet the impactor is released. The impactor is guided in a second tube of length 10 cm. At the end of this tube two laser beams are used to measure the speed of the impactor. This two-stage design ensures that the latex sheet is not perturbed by the gas ejected from the gun. The speed of the impactor can be adjusted with a pressure regulator.

The latex sheet stands horizontally on a net stretched on an open frame. The open frame is maintained approximately 10 cm below the end of the second tube by two electromagnets that are synchronized with the gas gun. When the electromagnets are switched off, two rubber bands violently pull the frame down and free the latex sheet. The latex sheet falls down under the action of gravity but the characteristic time scale of its fall is much longer than any other time scale in the problem. Thus, the impactor hits a perfectly free 'levitating' latex sheet. As discussed in §6*c*, the boundary conditions at the outer radius of the membrane do not play a crucial role in the study, and the main purpose of our set-up is to ensure that the latex sheet is stress-free when it is hit by the impactor.

The sheets are cut from natural latex rubber sheets of different thicknesses from 0.10 mm up to 0.30 mm. The radius of the sheets is typically $r_0=60$ mm. Static stretching tests reveal that in the range of stretching between 0 and 100 per cent, the elastic behaviour of the rubber remains linear (within 3%) with
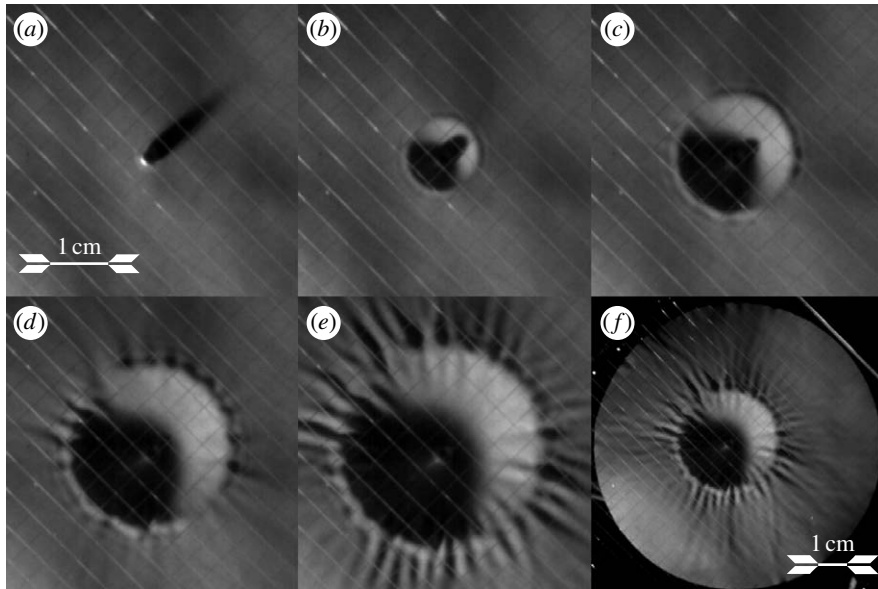
Figure 3. Bottom view of the impact of a steel ball of radius 2.25 mm on a thin rubber sheet of radius 55 mm and thickness 0.10 mm. The time step between two frames is 0.50 ms. $((a)–(c))$ As the ball impacts the sheet at speed $V=5.2\,\mathrm{m\,s^{-1}}$, the transverse wavefront propagates radially, $((c)–(e))$ material points are pulled towards the centre of the sheet and a circumferential compressive stress triggers a buckling instability selecting a well-defined wavelength, (f) zoomed out view of (e). A movie showing the dynamics is included in the electronic supplementary material.

a Young's modulus $E=1.5$ MPa and no significant hysteretic behaviour, i.e. stress softening of the rubber (Bouasse & Carrière 1903; Mullins 1947), is observed. In all our experiments the strain does not exceed 60 per cent. The density of the rubber is $\rho=990\,\mathrm{kg\,m^{-3}}$. The Poisson modulus is $\nu=0.5$ and thus the nominal wave speed for in plane disturbances is $c=\sqrt{E/\rho(1-\nu^2)}=45\,\mathrm{m\,s^{-1}}$.

Our diagnostics are based on quantitative image analysis, resolved in time. The typical time scale is $r_0/c\approx1.3$ ms. We use a Photron high-speed video camera to record movies at typical frame rates of 7000 up to 90 000 frames $\mathrm{s^{-1}}$. For side views, we use direct lighting with a black background. For movies showing a view from bottom a mirror is placed underneath the supporting device and the sheet is illuminated from above. When needed, regularly spaced marks are drawn on the sheet to follow the motion of the material points.

As a complement to document the impact phenomenology, we also conduct experiments using narrow latex strips instead of the circular latex sheets. The thickness of the strips is 0.10 mm, their length is 100 mm and their width is 4 mm.

3. Phenomenology

When a rigid body impacts the centre of the thin elastic disc at velocity V (figure 2a), a tensile front sets out from the impact point and propagates radially towards the edge of the sheet at speed of sound c. In the stretched area, material points move towards the centre of the sheet. As the impactor pulls the
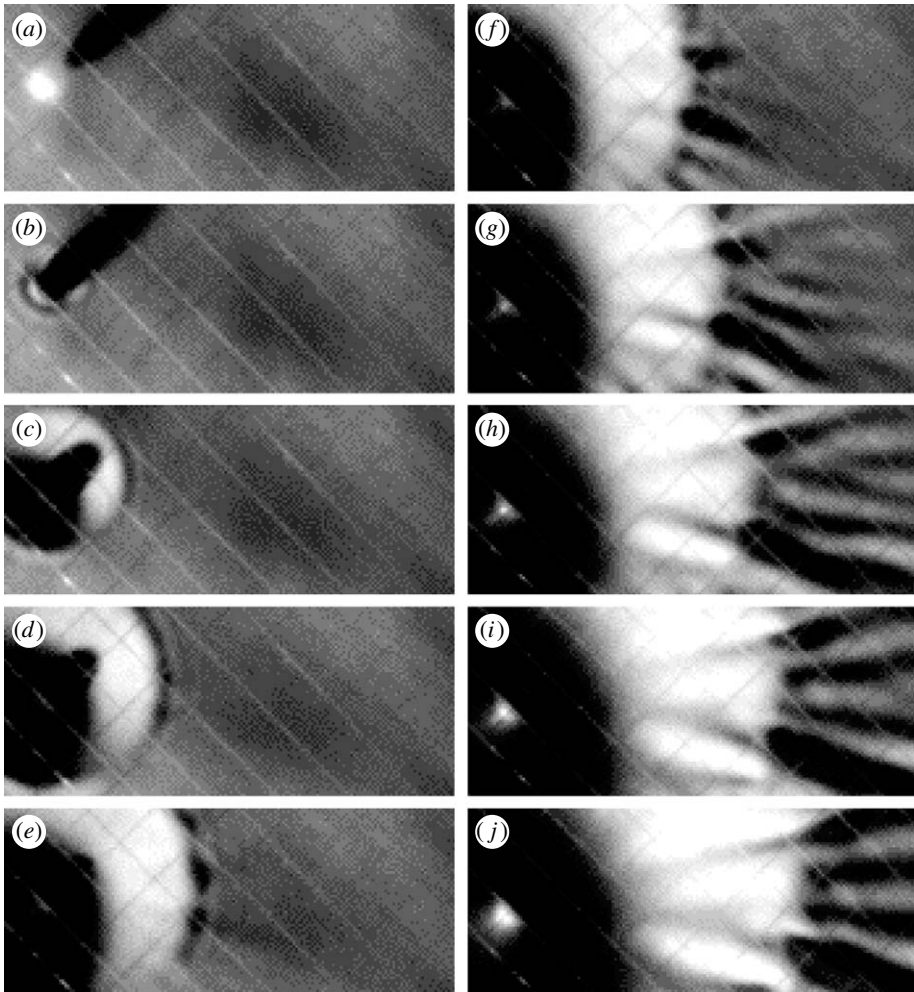
Figure 4. ((*a*)–(*j*)) Close bottom view of the transverse wavefront after impact of a steel ball at $V=5.2\,\mathrm{m\,s^{-1}}$ on a thin rubber sheet. Time goes by steps of 0.70 ms. Wrinkles appear at different stages so that the wavelength of the wrinkling pattern is constant.

membrane, with no observed sliding of the rubber against the impactor, a cone expands towards the edge of the sheet at velocity $\bar{U}$ (with $\bar{U} < c$) in the laboratory frame. In the stretched area, tensile stress in the radial direction is accompanied by contraction in the direction normal to it. Thus compressive circumferential stresses develop in the stretched area and the sheet buckles, giving rise to wrinkles (figure 3).

Experiments show that the buckling instability selects a wavelength rather than a number of folds. Indeed, as the transverse wavefront propagates the perimeter and width of the compressed area increase with time and so does the number of folds and thus the buckling wavelength does not change. As can be seen in figure 4, new folds are generated during the propagation of the transverse wavefront, so that the wavelength does not change with time.

We also study the one-dimensional version of the problem, the impact on a thin elastic strip (figure 2b). The phenomenology is similar except, de facto, for the formation of wrinkles: first a tensile front propagates away from the impact point and then, as the impacting body drags the strip out of its plane, a transverse 'V-shape' expands in the stretched material.

4. Wave propagation after impact

(a) *Wavefronts resulting from an impact on a one-dimensional elastic string*

An elastic string has a density ρ and Young's modulus E. The string length l is such that $l \gg ct$, in which $c = \sqrt{E/\rho}$ is the nominal wave speed for longitudinal disturbances (Love 1944) and t the typical time of observation after impact. The free string is impacted transversely at the point $x=0$. The mass of the impacting body is very large compared to the mass of the string, and the impacting velocity V is such that $V/c \ll 1$. In that limit, the projectile is not decelerated.

When the string is impacted, a longitudinal wave propagates at speed c. Behind the wavefront, the stretching ϵ (to be determined) is taken as constant and uniform. Material points are thus moving towards the impact point at speed $W = -c\epsilon$. In the stretched area, a transverse wave travels and a 'V-shaped' area expands (figure 2b). The base of this area travels at the speed of propagation of transverse disturbances. We assume that the stretching is ϵ also in the V-shaped area. In the frame of material points, the equation for the transverse displacement $\xi(x, t)$ is

$$\rho A \frac{\partial^2 \xi}{\partial t^2} = \frac{\partial(T \sin \phi)}{\partial x}, \tag{4.1}$$

where A is the cross section area and $T = EA\epsilon$ is the tension in the string. $\phi(x, t)$ is the angle between the local tangent and the x-axis and $(1+\epsilon)\sin \phi = \partial\xi/\partial x$. Thus the speed of transverse disturbances in the frame of material points is

$$U = c\sqrt{\frac{\epsilon}{1 + \epsilon}}. \tag{4.2}$$

At time t, the transverse wavefront reaches the material point $x_F = Ut$. This point has travelled a distance $W[t - t_l(x_F)]$ where $t_l(x_F) = x_F/c$ and thus its position in the laboratory frame is

$$\bar{x}_F = x_F - c\epsilon[t - t_l(x_F)] = x_F(1 + \epsilon) - c\epsilon t. \tag{4.3}$$

To relate the impactor speed with other quantities, we use Pythagoras' theorem

$$\bar{x}_F^2 + (Vt)^2 = (1 + \epsilon)^2 x_F^2. \tag{4.4}$$

Substituting $\bar{x}_F$, x_F and U, we obtain an equation for ϵ

$$\left[\sqrt{\epsilon(1 + \epsilon)} - \epsilon\right]^2 (ct)^2 + (Vt)^2 = \epsilon(1 + \epsilon)(ct)^2. \tag{4.5}$$

Interestingly, the leading contribution to the motion of the transverse wavefront is the motion of the material points towards the impact point at speed $-c\epsilon$. We obtain ϵ and the speed of the transverse wavefront in the laboratory frame $\bar{U} = \bar{x}_F/t$
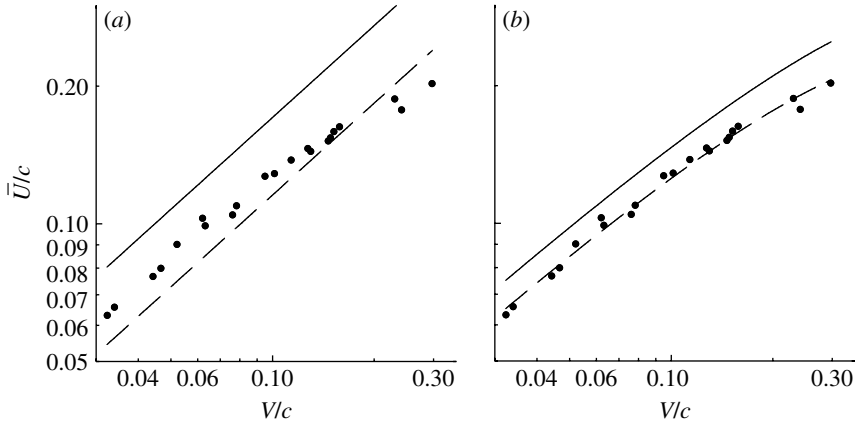
Figure 5. Transverse wavefront velocity in the laboratory frame versus impacting velocity, measured for a thin strip. The solid lines stand for the theoretical predictions with no adjustable parameter while the dotted lines stand for the fit with an adjusted prefactor. (*a*) First order in ϵ prediction, and (*b*) second order in ϵ prediction.

$$\epsilon = \left(\frac{V}{\sqrt{2}c}\right)^{4/3} + \left(\frac{V}{\sqrt{6}c}\right)^{2} + \mathcal{O}\big((V/c)^{2}\big), \qquad (4.6)$$

$$\frac{\bar{U}}{c} = \left(\frac{V}{\sqrt{2}c}\right)^{2/3} - \frac{5}{6}\left(\frac{V}{\sqrt{2}c}\right)^{4/3} + \mathcal{O}\big((V/c)^{2}\big). \qquad (4.7)$$

Figure 5 shows the measured dependence of the transverse wavefront velocity on the impacting velocity. Equation (4.7) agrees well with the measurements, but the theory overestimates the transverse-front velocity. This may come from the two-dimensional geometry of the latex rubber strips while we used a one-dimensional model for strings. Indeed, a careful examination of the images shows that the base of the cone connects smoothly rather than angularly with the straight section. This connection occurs over a length of a few millimetres (the width of the strip is 4 mm). Nevertheless, results clearly show that the mechanism we propose for the wavefront propagation after impact is the good scenario.

(*b*) *Waves resulting from an impact on a two-dimensional elastic membrane*

The problem of the impact on a circular membrane is more complicated because the circular waveforms do not maintain their shape as they propagate. The propagation mechanism is, however, the same as for the strings. As seen in figure 6, a tensile front propagates at the speed of sound in the material. Then a cone grows in a stretched area and thus it must obey the equation of propagation for transverse perturbations. Our objective here is to provide an approximate form for the stress field in the area of the tensile wave. This stress field will later be used to study the development of the wrinkling instability.

A circular elastic membrane has density ρ, Young's modulus E and Poisson ratio ν. The radius of the membrane is such that $r_0 \gg ct$, in which c given by $c^2 = E/[(1-\nu^2)\rho]$ is the nominal wave-speed for in plane disturbances and t is the
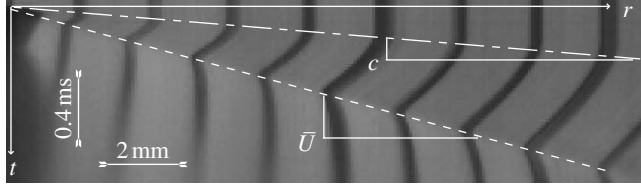
Figure 6. Space–time reconstruction of the motion of the material points on an impacted membrane taken from a high-speed movie. The longitudinal wavefront propagates at the speed of sound c. The transverse wavefront propagates at a constant speed $\bar{U}$ with $\bar{U} < c$.

typical time of observation after impact. The initially stress and strain-free membrane is transversely impacted at the point $r=0$. We consider that the mass of the impactor is much larger than the mass of the membrane, a limit for which the projectile deceleration can be neglected. The impacting velocity V is such that $V/c \ll 1$.

The radial displacement $\zeta(r, t)$ is given by the wave equation

$$\frac{1}{c^2}\frac{\partial^2 \zeta}{\partial t^2} = \frac{1}{r}\frac{\partial}{\partial r}\left(r\frac{\partial \zeta}{\partial r}\right) - \frac{\zeta}{r^2}. \tag{4.8}$$

This equation has no simple solution and we use a quasistatic approximation

$$\zeta(r, t) = \alpha(r_i + ct)\left(\frac{r}{r_i + ct} - \frac{r_i + ct}{r}\right), \tag{4.9}$$

where α is a dimensionless constant to be determined. The form for the displacement corresponds to the solution of the static problem with the boundary condition $\zeta=0$ at the tensile wavefront in $r=r_i+ct$. This solution cancels the right-hand side of equation (4.8). The radial strain is

$$\epsilon_r(r, t) = \frac{\partial \zeta}{\partial r} = \alpha\left(1 + \left(\frac{r_i + ct}{r}\right)^2\right), \tag{4.10}$$

and thus at the tensile wavefront $\epsilon_r = 2\alpha$. We measure the radial displacement by recording the motion of the regularly spaced marks drawn on the latex sheet. Figure 7 shows that the form of equation (4.9) fits the measurements.

The base of the cone propagates in a stretched area and we find experimentally that the propagation speed does not vary in time. Transverse displacements $\xi(r, t)$ for a membrane are ruled by

$$\rho\frac{\partial^2 \xi}{\partial t^2} = \frac{1}{r}\frac{\partial}{\partial r}(r\sigma_r \sin\phi), \tag{4.11}$$

where ϕ is the angle between a meridian line and the local tangent to the membrane in the radial direction and we have $\sin\phi \approx \partial\xi/\partial r$. The stresses are

$$\sigma_r = \frac{E}{1-\nu^2}(\epsilon_r + \nu\epsilon_\theta) \quad \text{and} \quad \sigma_\theta = \frac{E}{1-\nu^2}(\epsilon_\theta + \nu\epsilon_r), \tag{4.12}$$

where $\epsilon_r = \partial\zeta/\partial r$ is the radial strain and $\epsilon_\theta = \zeta/r$ the circumferential strain. The radial strain is positive while the circumferential strain is negative.
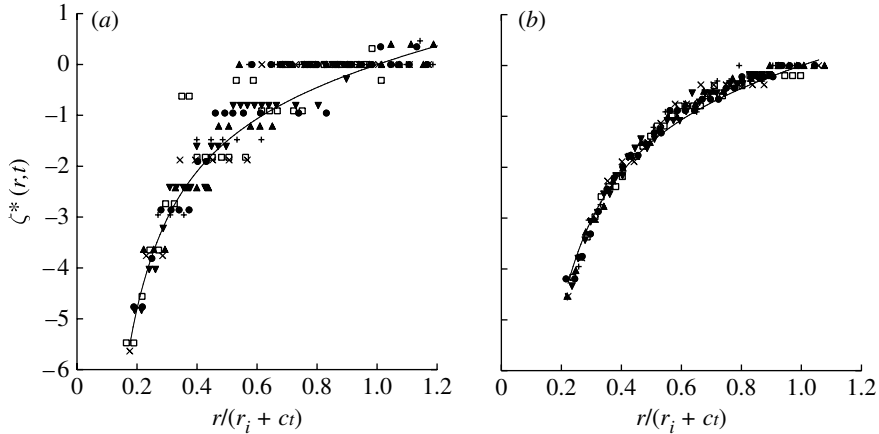
Figure 7. Radial displacement versus radial coordinate. We note $\zeta^*(r, t) = \zeta(r, t)/[\alpha(r_i + ct)]$. The solid line stand for the form given by (4.9) where the parameter α has been fitted. (a) Measurements performed for the impacting velocity $V = 12.8\ \mathrm{m\ s^{-1}}$ at different times after impact. Cross, 167 µs; plus, 222 µs; up-triangle, 278 µs; circle, 333 µs; square, 389 µs; down-triangle, 444 µs; and (b) measurements performed for the impacting velocity $V = 20.8\ \mathrm{m\ s^{-1}}$. Cross, 222 µs; plus, 278 µs; up-triangle, 333 µs; circle, 389 µs; square, 444 µs; down-triangle, 500 µs.

To relate the strain in the stretched domain with the speed of the impactor, we use the same geometrical argument as for the impacted string. The radial strain in the cone is taken as uniform and equal to $\epsilon_c = \epsilon_r(r_c, t)$. The geometrical relation is

$$(1 + \epsilon_c)^2 r_c^2(t) = (Vt)^2 + (\bar{U}t)^2, \tag{4.13}$$

where $r_c(t) = r_i + Ut$ is the (Lagrangian) coordinates of the transverse wavefront and $\bar{U}t = r_c(t) + \zeta(r_c, t)$ is the position of the wavefront in the laboratory frame. The right-hand side in equation (4.13) is based on the assumption that the membrane shape is conical, a good approximation as seen from figure 2a.

Assuming that the transverse wavefront is far from the impactor, i.e. $Ut \gg r_i$, we have

$$\zeta(r_c, t) = \alpha(r_i + ct)\left(\frac{r_i + Ut}{r_i + ct} - \frac{r_i + ct}{r_i + Ut}\right) \approx \alpha ct\left(\frac{U}{c} - \frac{c}{U}\right). \tag{4.14}$$

In this expression α and U are unknown. At the base of the cone, for large t, the radial strain deduced from the approximation for ζ is

$$\epsilon_c = \alpha\left[1 + \left(\frac{r_i + ct}{r_i + Ut}\right)^2\right] \approx \alpha\left[1 + \left(\frac{c}{U}\right)^2\right]. \tag{4.15}$$

When σ_r is constant in equation (4.11), transverse displacement waves propagate at speed $c_t = c\sqrt{\epsilon_r + \nu\epsilon_\theta}$ (e.g. Graff 1975). Thus we have

$$U = c\sqrt{\alpha\left(1 + \nu + (1 - \nu)\left(\frac{c}{U}\right)^2\right)}, \tag{4.16}$$
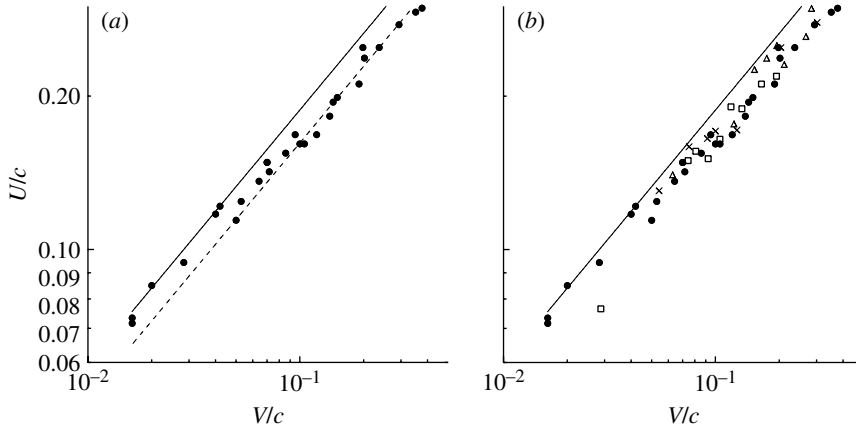
Figure 8. Transverse front velocity versus impact velocity. Velocity U in the lagrangian frame were deduced from the measurements of the transverse front velocity in the laboratory frame $\bar{U}$. (*a*) Measurements for a latex sheet of thickness $h=0.10$ mm. The solid line stands for the theoretical prediction with no adjustable parameter, the dashed line stands for the fit by the theoretical curve with an adjustable prefactor, we observe a 30% error on the prefactor. Thickness, $h=0.10$, and (*b*) measurements for latex sheet of different thicknesses. Circle, 0.10 mm; square, 0.15 mm; cross, 0.2 mm; up-triangle, 0.3 mm.

which gives

$$\alpha = \frac{\left(\frac{U}{c}\right)^4}{1-\nu+(1+\nu)\left(\frac{U}{c}\right)^2}. \tag{4.17}$$

In equation (4.13), we have at leading order

$$\left(1+\frac{2}{1-\nu}\left(\frac{U}{c}\right)^2\right)(Ut)^2 = (Ut)^2 - \frac{2}{1-\nu}\left(\frac{U}{c}\right)^2(Ut)^2 + (Vt)^2, \tag{4.18}$$

and thus

$$\frac{U}{c} = \left(\frac{1-\nu}{4}\right)^{1/4}\left(\frac{V}{c}\right)^{1/2}. \tag{4.19}$$

Figure 8 shows experimental measurements of the transverse wavefront versus impactor speed. The model that assumes $V/c\ll1$, overestimates the propagation speed but its dependence on the impacting speed is in good agreement with the experimental data. The model also assumes that $Ut\gg r_i$, but experiments show that the final speed of the transverse wavefront is reached for r very close to r_i (figure 6). The measurements conducted for different sheet thicknesses h show that the transverse front velocity does not depend on h for $0.10<h<0.30$ mm, as expected. For larger thicknesses, experiments reveal that the bending rigidity of the latex rubber sheet cannot be neglected, and discrepancies with the elastic membrane model are observed.
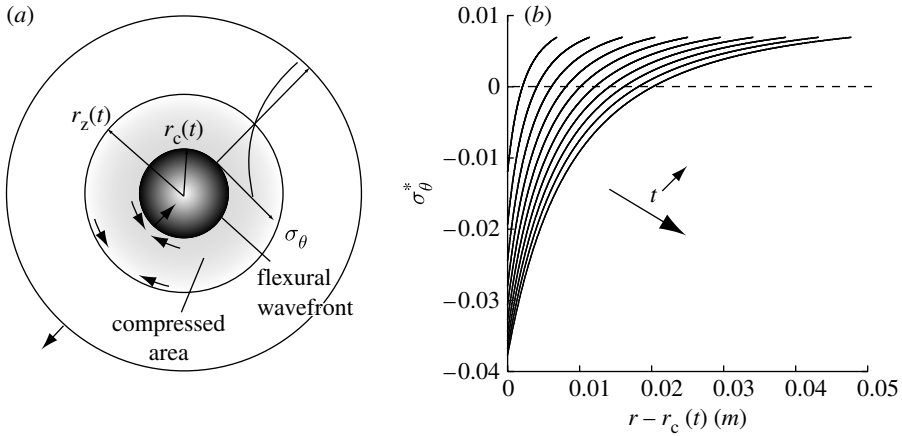
Figure 9. (*a*) Schematic showing the stress field in the stretched area consecutive to an impact on an elastic membrane. The central dark area is the cone. The shaded area represents the region $r_c(t) < r < r_z(t)$ where circumferential stress is compressive. (*b*) Variation of the normalized circumferential stress $\sigma_\theta^* = \sigma_\theta/(E/(1-\nu^2))$ with the distance to the transverse wavefront. The dashed line shows the position where the stress changes sign. The stresses are calculated for a membrane impacted at velocity $V=5\,\mathrm{m\,s^{-1}}$ by a 4.5 mm large impactor and for times ranging from 0.3 to 2.1 ms after impact.

(*c*) *Stress field resulting from an impact on a two-dimensional elastic membrane*

We use the approximation of equation (4.9) for the radial displacement to compute the stress field in the stretched area. With $\alpha=(1/4)(V/c)^2$, we have

$$\sigma_r(r, t) = \frac{E}{1-\nu^2}\left(\frac{V}{2c}\right)^2\left[1 + \nu + (1-\nu)\left(\frac{r_i + ct}{r}\right)^2\right], \qquad (4.20)$$

$$\sigma_\theta(r, t) = \frac{E}{1-\nu^2}\left(\frac{V}{2c}\right)^2\left[1 + \nu - (1-\nu)\left(\frac{r_i + ct}{r}\right)^2\right]. \qquad (4.21)$$

These expressions are valid in the domain between $r_c(t)=r_i + Ut$ and $r_t(t)= r_i + ct$. The circumferential stress becomes negative at $r=r_z(t)=[(1-\nu)/(1+\nu)]^{1/2}(r_i+ct)$. Then the area of the plate delimited by the transverse wavefront $r=r_c(t)$ and $r=r_z(t)$ is compressed along the circumferential direction (figure 9). This compression results from a geometrical constrain: consider two points initially at radius r and at angles θ_1 and θ_2. Initially, the arc length between these two points is $r(\theta_2-\theta_1)$. After deformation this distance is reduced to $[r+\zeta(r,t)](\theta_2-\theta_1)$ where $\zeta(r, t)$ is negative.

5. Dynamic wrinkling

In thin sheets, in-plane compressive stresses lead to the formation of wrinkles. In this section, we study the appearance of wrinkles and we compute their size. As usual for buckling instabilities, this size results from a balance between destabilization induced by the circumferential compression, and restoring forces

due to the sheet bending rigidity. To model the behaviour of the compressed area, we investigate the analogue problem of the stability of an annular plate, of inner radius $r_c(t)$ and outer radius $r_z(t)$, to which is applied the in-plane stress field (both radial and circumferential) found in §4c. The problem is similar to the static problem studied by Géminard *et al.* (2004). Coman & Haughton (2006) also proposed a theoretical analysis of the problem. These authors studied the stability of the plan solution and computed the shape of the unstable mode as a function of r and θ. We adopt a global method imposing the shape of the pattern, providing the instability threshold and azimuthal wavelength. Later on, we also discuss a simplified model, approximating the annulus with a beam, resembling the method used by Senior (1956) in the context of wrinkling in metal punching but with added inertia.

(a) Instability of the stretched membrane

The Rayleigh method (Rayleigh 1894) is an application of the least-action principle to vibrating systems whose dynamics is on purpose restricted to one degree of freedom. The method consists in making the inventory of the elastic energies involved, namely the bending energy U_b, the circumferential compressive energy U_c, the radial tensile energy U_t, construct a potential $U = U_b + U_c + U_t$ and then write

$$\delta \int \mathrm{d}t (T - U) = 0, \tag{5.1}$$

where T is the sheet kinetic energy, and δ stands for a variation in the displacements ξ_n that make the integral minimum. The optimum provides the dispersion relation of the problem for given in-plane stresses σ_r and σ_θ. We consider a single radial bent, imposing $\xi = 0$ at the inner radius $r = r_c(t)$ and outer radius $r = r_z(t)$ and account for n folds in the circumferential direction as

$$\xi(r, \theta, t) = \frac{(r - r_c)(r - r_z)}{(r_z - r_c)^2} \xi_n \sin(n\theta) \, \mathrm{e}^{\gamma_n t}, \tag{5.2}$$

where ξ_n and γ_n are, respectively, the amplitude and the growth rate. This form assumes that the out of plane displacement for $r > r_z$ is zero.

— The expression for the bending energy is

$$U_b = \frac{D}{2} \int_0^{2\pi} \int_{r_c}^{r_z} \left\{ \left(\frac{\partial^2 \xi}{\partial r^2} + \frac{1}{r} \frac{\partial \xi}{\partial r} + \frac{1}{r^2} \frac{\partial^2 \xi}{\partial \theta^2} \right)^2 - 2(1-v) \left(\frac{\partial^2 \xi}{\partial r^2} \right) \left(\frac{1}{r} \frac{\partial \xi}{\partial r} + \frac{1}{r^2} \frac{\partial^2 \xi}{\partial \theta^2} \right) \right.$$

$$\left. + 2(1-v) \left(\frac{\partial}{\partial r} \left(\frac{1}{r} \frac{\partial \xi}{\partial \theta} \right) \right)^2 \right\} r \, \mathrm{d}r \, \mathrm{d}\theta, \tag{5.3}$$

where $D = Eh^3/[12(1-v^2)]$ is the bending rigidity (Timoshenko & Woinowsky-Krieger 1959). With ξ given by equation (5.2), the bending energy writes

$$U_b = \frac{\pi D \xi_n^2 \, \mathrm{e}^{2\gamma_n t}}{2(r_z - r_c)^4} \left\{ \left[-3(r_z^2 - r_c^2) + (r_c^2 + 4r_c r_z + r_z^2) \ln \frac{r_z}{r_c} \right] n^4 \right.$$

$$\left. + 2 \left[4(r_z^2 - r_c^2) - (r_c^2 + 6r_c r_z + r_z^2) \ln \frac{r_z}{r_c} \right] n^2 + \left[(r_c + r_z)^2 \ln \frac{r_z}{r_c} \right] \right\}. \tag{5.4}$$

— In-plane stresses also contribute to the elastic energy of the system. The compressive circumferential stress σ_θ yields a compressive energy U_c while the radial stress σ_r yields a tension energy U_t. They are given by

$$U_c = \frac{h}{2} \int_0^{2\pi} \int_{r_c}^{r_z} \left\{ \sigma_\theta \left(\frac{1}{r} \frac{\partial \xi}{\partial \theta} \right)^2 \right\} r \, dr \, d\theta, \tag{5.5}$$

$$U_t = \frac{h}{2} \int_0^{2\pi} \int_{r_c}^{r_z} \left\{ \sigma_r \left(\frac{\partial \xi}{\partial r} \right)^2 \right\} r \, dr \, d\theta. \tag{5.6}$$

The compressive and tensile energies thus write

$$U_c = \frac{\pi D \xi_n^2 \, e^{2\gamma_n t} n^2}{2h^2 (r_c - r_z)^4} \left(\frac{V}{2c} \right)^2 I_c, \tag{5.7}$$

$$U_t = \frac{\pi D \xi_n^2 \, e^{2\gamma_n t}}{h^2 (r_c - r_z)^4} \left(\frac{V}{2c} \right)^2 I_t, \tag{5.8}$$

with

$$I_c = \frac{1}{2} \left\{ (1-\nu)(r_i + ct)^2 \left[36(r_z^2 - r_c^2) - 12(r_z^2 + 4r_c r_z + r_c^2) \ln \frac{r_z}{r_c} \right] \right.$$
$$\left. + (1+\nu) \left[12 r_c^2 r_z^2 \ln \frac{r_z}{r_c} + (r_z^2 - r_c^2)(r_c^2 - 8r_c r_z + r_z^2) \right] \right\}, \tag{5.9}$$

and

$$I_t = (1-\nu)(r_i + ct)^2 \left[6(r_c + r_z)^2 \ln \frac{r_z}{r_c} - 12(r_z^2 - r_c^2) \right] + (1+\nu)\left(r_z^2 - r_c^2 \right)^2. \tag{5.10}$$

— Finally, the kinetic energy is given by

$$T = \frac{\rho h}{2} \int_0^{2\pi} \int_{r_c}^{r_z} \left\{ \left(\frac{\partial \xi}{\partial t} \right)^2 \right\} r \, dr \, d\theta. \tag{5.11}$$

Using $\rho = 12D/(c^2 h^3)$, we have

$$T = \frac{\pi D \xi_n^2 \gamma_n^2 \, e^{2\gamma_n t}}{10 c^2 h^2} \left(r_z^2 - r_c^2 \right). \tag{5.12}$$

Then, using (5.1), we find the dispersion equation for the circumferential wavenumber n. In terms of the dimensional circumferential wavenumber calculated at the inner radius $k_n = n/r_c$, the dispersion relation reads

$$\frac{(r_z - r_c)^4 (r_z^2 - r_c^2)}{10 c^2 h^2} \gamma_n^2 + \frac{1}{2} k_n^4 r_c^4 \left[-3(r_z^2 - r_c^2) + (r_c^2 + 4r_c r_z + r_z^2) \ln \frac{r_z}{r_c} \right]$$
$$+ k_n^2 r_c^2 \left[4(r_z^2 - r_c^2) - (r_c^2 + 6r_c r_z + r_z^2) \ln \frac{r_z}{r_c} + \frac{1}{2} \left(\frac{V}{2c} \right)^2 \frac{I_c}{h^2} \right]$$
$$+ \frac{1}{2} (r_c^2 + r_z^2) \ln \frac{r_z}{r_c} + \left(\frac{V}{2c} \right)^2 \frac{I_t}{h^2} = 0. \tag{5.13}$$
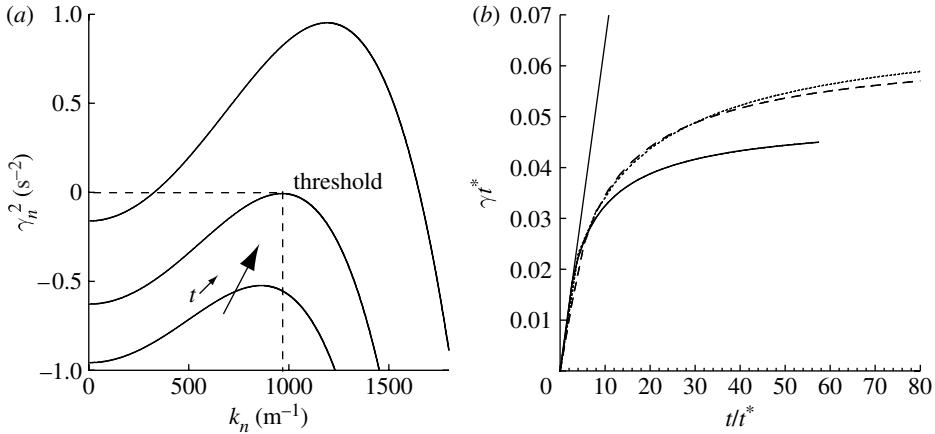
Figure 10. (*a*) Variation of the instability growth rate with the wavenumber. The dispersion relation was calculated numerically for a projectile of radius $r_i = 2.25$ mm impacting a plate of thickness $h = 0.15$ mm at impacting velocity $V = 10$ m s^{-1}. The dispersion relation is calculated for several times after impact: 300 μs, 365 μs and 700 μs. We observe a finite wavenumber at the instability threshold. (*b*) Time evolution of the maximal growth rate γ as a function of time. Times are normalized by $t^* = h/v$; $h = 0.15$ mm. Solid line, $V = 5$ m s^{-1}; dashed line, $V = 10$ m s^{-1}; dotted line, $V = 15$ m s^{-1}.

The second term (proportional to k_n^4) is always positive and thus at short wavelength, γ_n^2 is negative and the solution is stable. The source of the instability is the term proportional to I_c. Substituting time dependence for the radius r_z and r_c, we obtain a dispersion equation dependent on time (figure 10). At a critical time t_{inst}, the sign of γ_n^2 changes and the axisymmetric solution becomes unstable. A wavelength is selected by the instability.

The critical time at which the axisymmetric solution becomes unstable can be computed by looking for a double root of the equation in k_n obtained by looking at solutions $\gamma_n = 0$. A wavelength is associated with this critical time. Comparison between the wavelength computed from equation (5.13) and the experimental wavelength shows a good agreement (figure 11). However, for very thin sheets and high-impacting speeds (figure 11*a*), the instability develops at early times and the approximation $r \gg r_i$ used to obtain equation (4.19) is no longer valid.

We also measured the time at which we started to observe wrinkling (figure 12). This time is not *stricto sensu* equal to t_{inst} because the wrinkles need time to grow, whereas at the instability threshold (i.e. at time t_{inst}), the growth rate is zero. Above t_{inst}, the maximal growth rate γ increases itself in time (figure 10*b*) and saturates over a time period of approximately 10 h/V. Figure 12 shows that the typical wrinkling time is indeed $t_{inst} + 10$ h/V.

(*b*) *Approximation of the instability wavelength*

An explicit form for the critical time t_{inst} and the instability wavelength λ cannot be easily computed from equation (5.13). In the limit $r_i \to 0$ and assuming that V/c is small, the instability occurs at large times. The compressed area
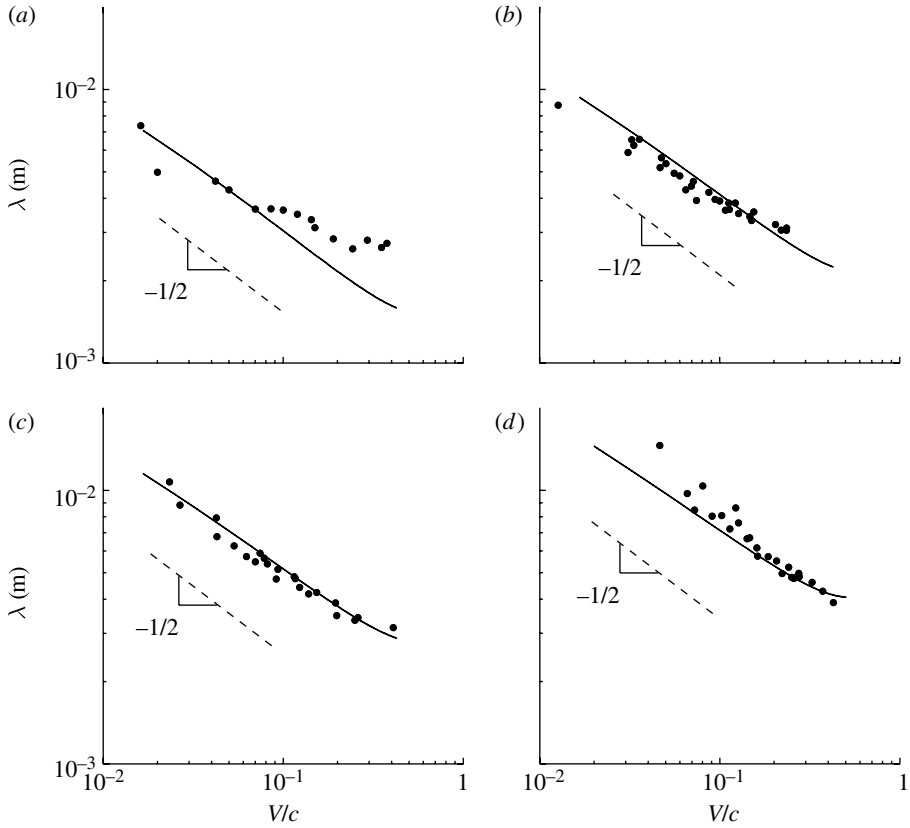
Figure 11. ((*a*)–(*d*)) Variation of the buckled wavelength with the impacting velocity. We conducted experiments with a projectile of radius $r_i = 2.25$ mm and latex sheets of different thicknesses. The solid lines stand for the theoretical predictions with no adjustable parameter. (*a*) $h=0.10$ mm; (*b*) $h=0.15$ mm; (*c*) $h=0.20$ mm; (*d*) $h=0.30$ mm.

shown in figure 9 has a large radius and its curvature can be neglected, hence, we propose the following toy model to understand the instability mechanism: consider an elastic beam of length $\pi[r_z(t)+r_c(t)]$ and width $b=r_z(t)-r_c(t)$ with a compression

$$\sigma_c = \sigma_\theta(r_c) = \frac{E}{1-\nu^2}\left(\frac{V}{2c}\right)^2\left[(1+\nu)-2\sqrt{1-\nu}\,\frac{c}{V}\right] \approx -\frac{E}{1-\nu^2}\sqrt{1-\nu}\,\frac{V}{2c}. \quad (5.14)$$

The dispersion equation (Lindberg 1965; Vermorel *et al.* 2007) is

$$\omega^2 = \frac{EI}{\rho bh}k^2\left\{k^2 + \sigma_c\frac{bh}{EI}\right\}, \quad (5.15)$$

where $I=bh^2/12$ is the area moment of inertia. The straight configuration of the beam is unstable and a dynamic buckling instability develops. This instability selects a most amplified wavelength

$$\lambda_{\max} = \pi h\sqrt{\frac{2}{3}}\sqrt{\frac{E}{|\sigma_c|}} \approx \frac{2\sqrt{3}}{3}\pi(1+\nu)^{1/2}(1-\nu)^{1/4}h\left(\frac{V}{c}\right)^{-1/2}. \quad (5.16)$$
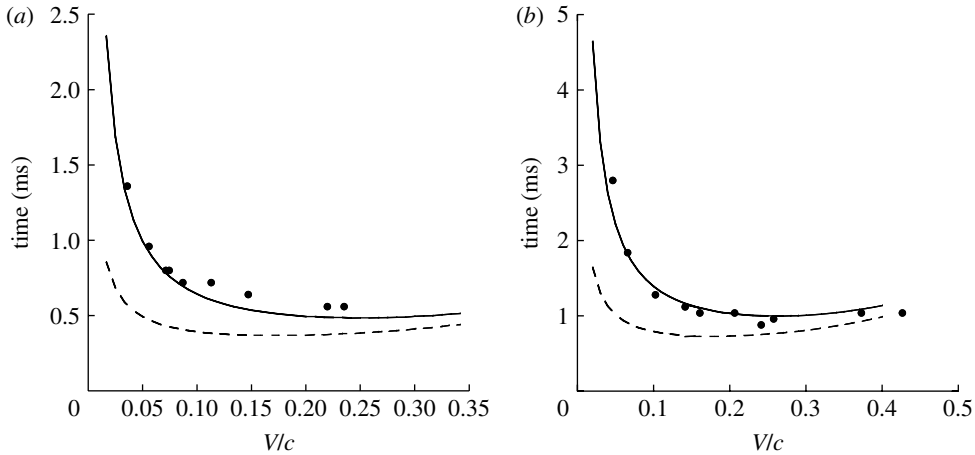
Figure 12. Development time of the wrinkling instability observed experimentally as a function of the impacting velocity. Dashed line, contribution of t_{inst} only; solid line, $t_{inst} + 10h/V$ (see text). (*a*) $h = 0.15$ mm; (*b*) $h = 0.30$ mm.

The scaling above $\lambda \propto h(V/c)^{-1/2}$ is precisely the one observed experimentally for moderately thin sheets (figure 11). The instability time of growth is

$$\tau_{growth} = \frac{\sqrt{3}}{3} h \frac{1}{c} \frac{E}{|\sigma_c|} \approx 2 \frac{\sqrt{3}}{3} (1 - \nu^2) \frac{h}{V}, \tag{5.17}$$

whose scaling again recovers that of t_{inst}.

6. Conclusion and discussion

(*a*) *Summary*

We have shown that a transversely impacted thin sheet experiences a buckling instability leading to the growth of radial wrinkles. The instability results from a 'geometrical confinement' of the material points that are pulled by the impactor towards the impact point. The wavelength is correctly predicted by a quasistatic analysis of a time-varying substrate. Interestingly, this instability is not observed in clamped circular sheets with a central transverse force. On the other hand, this instability occurs in membranes that are geometrically constrained at one or two different radii as in Géminard *et al.* (2004), Huang *et al.* (2007) or Chopin *et al.* (2008). The necessary confinement occurs in the present case because the tensile wavefront propagates faster than the transverse wavefront. The main difference with the static case concerns the wrinkle pattern: in the static case, a number of wrinkles are selected and the wavelength changes with the distance from the centre while here the wavelength is conserved.

We also note the similarity between the patterns resulting from this wrinkling instability and the cracks that are observed on impacted plates of brittle materials, whose analysis is left for future work.

Modification of geometry, boundary conditions, impact parameters or material properties may only modify the critical radius (and critical time) at which the instability develops. Thus, our model does not predict a threshold for the

buckling instability. In the following, we discuss different limitations of our model. In particular, we discuss the effects of the inertia of the impactor and of the size and thickness of the latex sheet.

(b) Deceleration of the impacting body

We assumed that the velocity of the impactor V does not change during impact. If the mass of the impactor is finite, however, it decelerates. Using the results of §4b, the rate of decrease of the impactor's velocity can be estimated from momentum conservation of the system composed of the impactor and the mass of the membrane displaced vertically.

Consider a rigid impactor of mass M_p, impacting an elastic sheet at initial impacting velocity V. The part of the sheet whose motion is vertical is the area delimited by the transverse wavefront resulting from impact. The vertical velocity of the membrane at the impact point is the same as the impactor current velocity $v(t)$. As an approximation, we consider that the transverse wavefront velocity depends only on the initial impacting velocity V as if the impactor had an infinite mass and we use the result from (4.19). Then, the mass of the membrane moving vertically is

$$M_m = \rho h \pi (Ut)^2 = \pi \rho h \left(\frac{1-\nu}{4}\right)^{1/2} \left(\frac{V}{c}\right) c^2 t^2. \tag{6.1}$$

Conservation of momentum in the vertical direction writes as

$$\frac{d}{dt}\{(M_p + M_m)v\} = (M_p + M_m)\frac{dv}{dt} + v\frac{dM_m}{dt} = 0. \tag{6.2}$$

Hence the differential equation satisfied by $v(t)$

$$\frac{dv}{dt} = -\left(\frac{2t}{t^2 + \tau^2}\right)v, \quad \text{with} \quad \tau^2 = \frac{M_p}{\pi \rho h \left(\frac{1-\nu}{4}\right)^{1/2} \left(\frac{V}{c}\right) c^2}, \tag{6.3}$$

which integrates into

$$v(t) = \frac{V}{1 + (t/\tau)^2}. \tag{6.4}$$

Measurements of the impactor velocity $v(t)$ and of the characteristic deceleration time τ shown in figure 13 are in a good agreement with equation (6.4). The typical observation time in the present experiments does not exceed 2 ms after the time of impact. The mass of the impactor associated to $\tau = 2$ ms for a membrane thickness $h = 0.30$ mm and for an impacting velocity $V = 30$ m s^{-1} is $M_p = 2.4 \times 10^{-3}$ kg. The experiments presented in this work were all conducted with $M_p = 3.3 \times 10^{-3}$ kg or larger, masses for which deceleration does not alter our conclusions.

(c) Finite size effects

According to the dispersion equation (5.13), the instability develops for any impacting speed. However, finite size limitations can modify the dynamics. The tension front reaches the extremity of the sheet in $r = r_0$ at time $t_0 = r_0/c$.
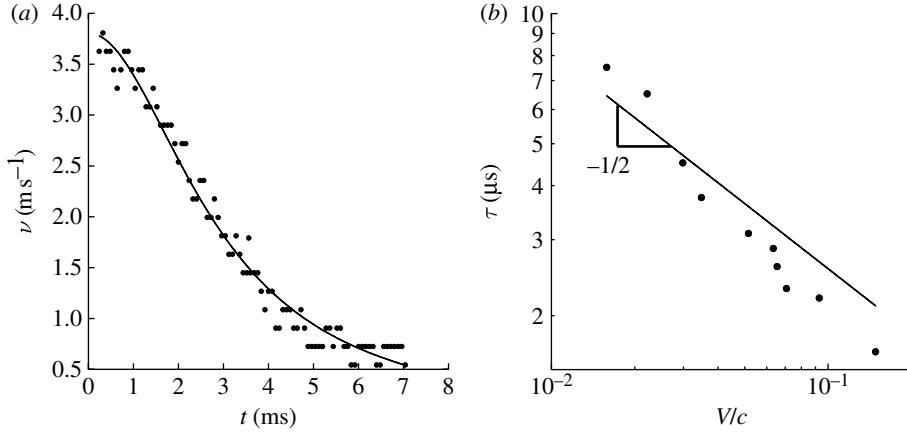
Figure 13. (*a*) Variation of the velocity of the impactor (a steel ball of mass $M_p = 0.33 \times 10^{-3}$ kg) with time. The solid line stands for the fitting curve with one adjustable parameter evaluating the characteristic time τ. The data fit provides $\tau = 2.92$ ms while the theoretical value is 2.9 ms. $h = 0.15$ mm; $V = 3.8$ m s^{-1}, and (*b*) variation of the characteristic time τ with the impacting velocity. The solid line stands for the fit by the theoretical power law $(V/c)^{-1/2}$. The error on the prefactor does not exceed 10 per cent. $h = 0.15$ mm.

This front rebounds and if it reaches the position $r = r_z$ before the development of the instability, the stress field changes, and we expect a modified dynamics. Thus the critical size for the membrane is given by the criterion

$$\frac{r_i - r_0}{c} + \frac{r_0 - r_z(t_{inst})}{c} < t_{inst}. \tag{6.5}$$

The measurements in the present experiments (wave speed, radial displacements, wavelengths) were performed before perturbation by the rebounding front. We also note that the shape of the rebounding front depends on the boundary conditions (free, clamped). However, as long as there is no interaction with the rebounding wavefronts, the boundary conditions do not influence the dynamics and the development of the instability. This is a difference with the static situation where the boundary conditions are fundamental in predicting the onset of wrinkling.

(*d*) *Pure bending waves*

Finally, our model for transverse wave propagation disregards the dynamics of pure bending waves, decoupled from tension in the sheet. We briefly discuss the validity of this model in the one-dimensional case. If flexural stiffness is taken into account equation (4.1) now reads

$$EAr^2 \frac{\partial^4 \xi}{\partial x^4} + \frac{\partial}{\partial x}\left(T\frac{\partial \xi}{\partial x}\right) + \rho A \frac{\partial^2 \xi}{\partial t^2} = 0, \tag{6.6}$$

where r is the radius of gyration of the beam ($r^2 = h^2/12$ for a rectangular cross section of thickness h) and $T = EA\epsilon$. We note that this equation is valid at times larger than h/c. When the beam is impacted, transverse waves propagate as

bending waves and tension increases gradually as a consequence of transverse motion. Consequently, any localized disturbance, say $\xi(r, t=0) = f(r)$, will propagate according to (6.6) as a wave packet $\xi(r, t) = F(r/\sqrt{\kappa t})$, where $\kappa = cr$ and $F(\cdot)$ is an eigenfunction of (6.6) (e.g. Graff 1975). The wave packet thus expands over a typical width increasing as $\sqrt{\kappa t}$. Now, the tension front sustained by the continuing traction of the impactor has propagated radially over a distance ct at time t. Thus assuming that the tensile strain is uniform over the stretched domain, we estimate the strain in the beam as follows: the segment of initial length ct now has a length of $ct - \sqrt{\kappa t} + [\kappa t + (Vt)^2]^{1/2}$ and thus the strain is

$$\epsilon = \frac{ct - \sqrt{\kappa t} + [\kappa t + (Vt)^2]^{1/2} - ct}{ct} \approx \frac{1}{2}\left(\frac{V}{c}\right)^2 \frac{ct}{\sqrt{\kappa t}}. \qquad (6.7)$$

Using this estimate, we compare the two first terms in equation (6.6): the bending term writes $EAr^2(Vt)/(\kappa t)^2$ and the tension term writes $EA(V/c)(ct/\sqrt{\kappa t})Vt/\kappa t$. Thus the bending term dominates until a critical time

$$t_{\rm b} = \frac{r}{V}\left(\frac{c}{V}\right)^{1/3} \propto \frac{h}{V}\left(\frac{c}{V}\right)^{1/3}, \qquad (6.8)$$

above which the restoring force due to tension overcomes the intrinsic bending rigidity. This time is greater than h/V and thus the impactor must have travelled a distance greater than h for the tension to be large enough. In two dimensions, we expect the same limitation but in our experiments h/V (typically 10^{-5} s) is very short compared to observation times; our model neglecting bending rigidity is valid.

References

Backman, M. A. & Goldsmith, W. 1978 The mechanics of penetration of projectiles into target. *Int. J. Eng. Sci.* **16**, 1–99. (doi:10.1016/0020-7225(78)90002-2)

Begley, M. R. & Mackin, T. J. 2004 Spherical indentation of freestanding circular thin films in the membrane regime. *J. Mech. Phys. Solids* **52**, 2005–2023. (doi:10.1016/j.jmps.2004.03.002)

Bouasse, H. & Carrière, Z. 1903 Sur les courbes de traction du caoutchouc vulcanisé. *Annales de la faculté des sciences de Toulouse, 2e série* **5**, 257–283.

Cerda, E., Mahadevan, L. & Pasini, J. M. 2004 The elements of draping. *Proc. Natl Acad. Sci. USA* **101**, 1806–1810. (doi:10.1073/pnas.0307160101)

Chopin, J., Vella, D. & Boudaoud, A. 2008 The liquid blister test. *Proc. R. Soc. A* **464**, 2887–2906. (doi:10.1098/rspa.2008.0095)

Coman, C. D. & Haughton, D. M. 2006 Localized wrinkling instabilities in radially stretched annular thin films. *Acta Mech.* **185**, 179–200. (doi:10.1007/s00707-005-0307-2)

Géminard, J.-C., Bernal, R. & Melo, F. 2004 Wrinkle formations in axi-symmetrically stretched membranes. *Eur. Phys. J. E* **15**, 117–126. (doi:10.1140/epje/i2004-10041-1)

Graff, K. G. 1975 *Wave motion in elastic solids.* New York, NY: Dover Publications.

Huang, J., Juszkiewicz, M., de Jeu, W.H, Cerda, E., Emrick, T., Menon, N. & Russell, T. P. 2007 Capillary wrinkling of floating thin polymer films. *Science* **317**, 650–653. (doi:10.1126/science.1144616)

Lindberg, H. E. 1965 Impact buckling of a bar. *J. Appl. Mech.* **32**, 315–322.

Love, A. E. H. 1944 *A treatise on the mathematical theory of elasticity*, 4th edn. New York, NY: Dover Publications.

Mullins, L. 1947 Effect of stretching on the properties of rubber. *J. Rubber Res.* **16**, 275–289.

Phoenix, S. L. & Porwal, P. K. 2003 A new membrane model for the ballistic impact response and V50 performance of multi-ply fibrous systems. *Int. J. Solids Struct.* **40**, 6723–6765. (doi:10.1016/S0020-7683(03)00329-9)

Rayleigh, J. W. S. 1894 *The theory of sound.* New York, NY: Dover Publications.

Senior, B. W. 1956 Flange wrinkling in deep-drawing operations. *J. Mech. Phys. Solids* **4**, 235–246. (doi:10.1016/0022-5096(56)90032-1)

Timoshenko, S. & Woinowsky-Krieger, S. 1959 *Theory of plates and shells.* New York, NY: McGraw-Hill.

Vermorel, R., Vandenberghe, N. & Villermaux, E. 2007 Rubber band recoil. *Proc. R. Soc. A* **463**, 641–658. (doi:10.1098/rspa.2006.1781)